The Journal of Immunology

Macrophages Guard Endothelial Lineage by Hindering Endothelial-to-Mesenchymal Transition: Implications for the Pathogenesis of Systemic Sclerosis

Pier Andrea Nicolosi, Enrico Tombetti, Anna Giovenzana, Eleonora Donè, Eleonora Pulcinelli, Raffaella Meneveri, Mario Tirone, Norma Maugeri, Patrizia Rovere-Querini, Angelo A. Manfredi and Silvia Brunelli

J Immunol 2019; 203:247-258; Prepublished online 24 May 2019;
doi: 10.4049/jimmunol.1800883
http://www.jimmunol.org/content/203/1/247

The Journal of Immunology is published twice each month by
The American Association of Immunologists, Inc.,
1451 Rockville Pike, Suite 650, Rockville, MD 20852

Print ISSN: 0022-1767 Online ISSN: 1550-6606.

Macrophages Guard Endothelial Lineage by Hindering Endothelial-to-Mesenchymal Transition: Implications for the Pathogenesis of Systemic Sclerosis

Pier Andrea Nicolosi,* Enrico Tombetti,† Anna Giovenzana,* Eleonora Donè,* Eleonora Pulcinelli,* Raffaella Meneveri,* Mario Tirone,*,‡ Norma Maugeri,† Patrizia Rovere-Querini,†,§ Angelo A. Manfredi,†,§ and Silvia Brunelli*

The signals that control endothelial plasticity in inflamed tissues have only been partially characterized. For example, it has been shown that inadequate vasculogenesis in systemic sclerosis (SSc) has been associated with an endothelial defect. We used a genetic lineage tracing model to investigate whether endothelial cells die or change phenotypically after fibrosis induction and whether signals released by cells of the innate immune system and in the blood of patients influence their commitment. We observed that in the lineage-tracing transgenic mice Cdh5-CreER^{T2}::R26R-EYFP, endothelial-derived cells (EdCs) underwent fibrosis after treatment with bleomycin, and EdCs retrieved from the lung showed expression of endothelial-to-mesenchymal transition (EndoMT) markers. Liposome-encapsulated clodronate was used to assess macrophage impact on EdCs. Clodronate treatment affected the number of alternatively activated macrophages in the lung, with upregulated expression of EndoMT markers in lung EdCs. Endothelial fate and function were investigated in vitro upon challenge with serum signals from SSc patients or released by activated macrophages. Sera of SSc patients with anti-Scl70 Abs, at higher risk of visceral organ fibrosis, induced EndoMT and jeopardized endothelial function. In conclusion, EdCs in SSc might be defective because of commitment to a mesenchymal fate, which is sustained by soluble signals in the patient's blood. Macrophages contribute to preserve the endothelial identity of precursor cells. Altered macrophage-dependent plasticity of EdCs could contribute to link vasculopathy with fibrosis. ***The Journal of Immunology*****, 2019, 203: 247–258.**

Systemic sclerosis (SSc) is a systemic disease characterized by noninflammatory vasculopathy, immunological alteration, and dysregulated fibrotic response (1). Fibrosis interferes with the architecture and the function of tissues and organs, including the lung, and is responsible of the increased mortality and the elevated morbidity (2).

Early SSc events involve the microcirculation and small arterioles (3). Endothelial cells undergo activation and apoptosis, perivascular tissues are infiltrated by leukocytes, whereas pericytes and smooth muscle cells proliferate (4–7). The microvascular damage results in hypoxia and oxidative stress (8) and defective angiogenesis and vasculogenesis amplify and sustain myofibroblasts activation and fibrogenesis (5, 9, 10).

Endothelial cells orchestrate the function and provide metabolites for epigenetic regulation of vascular cells (11). Disturbed angiogenesis, vascular tone, and myofibroblast generation/functional activation are consequences of endothelial insufficiency (12). Endothelial progenitors adapt to environmental conditions by yielding diverse progenies (13, 14). As part of this plasticity, endothelial progenitors and their progeny, endothelial-derived cells (EdCs) lose their endothelial specification and acquire mesenchymal characteristics. This process referred to as endothelial-to-mesenchymal transition (EndoMT) contributes to organ development, remodeling, and fibrosis (15, 16). Numerical and functional defects of endothelial cells contribute to the failure of SSc vessels to cope with damage (17–19). EndoMT has been suggested to play a role in role in dermal fibrosis, based on evidences obtained on skin sections of SSc patients studied by immunofluorescence (IF) and in experimental mouse models of fibrosis (20).

Macrophages influence the function and molecular repertoire of endothelial cells, while counteracting EndoMT in a model of muscle repair after sterile injury (21) and preventing fibrosis, which is the outcome of wound healing in their absence (21). Infiltrating macrophages are commonly found interspersed between SSc collagen fibers and areas surrounding vessels (22, 23). Macrophages are thought to contribute to the maladaptive remodeling in SSc because they can, after alternative activation, sustain myofibroblast fitness and function via mechanisms that are still unidentified (22, 24). We reasoned that the kinetics of macrophage infiltration of murine tissues undergoing fibrosis and their presence

*School of Medicine and Surgery, University of Milano-Bicocca, 20900 Monza, Italy; †Division of Immunology, Transplantation and Infectious Disease, IRCCS San Raffaele Scientific Institute, 20132 Milan, Italy; ‡Division of Genetics and Cell Biology, IRCCS San Raffaele Scientific Institute, 20132 Milan, Italy; and §Università Vita-Salute San Raffaele, 20132 Milan, Italy

ORCIDs: 0000-0002-3889-456X (A.G.); 0000-0003-0791-5951 (R.M.); 0000-0003-3931-0412 (N.M.); 0000-0003-1753-5346 (S.B.).

Received for publication June 25, 2018. Accepted for publication April 23, 2019.

This work was supported by grants from Università Milano-Bicocca (FAR-QC2014 and FAR 2014-2016 to S.B.) and by the "Irene Tassara" award of the Associazione Italiana Lotta alla Sclerodermia (to A.A.M.).

Address correspondence and reprint requests to Prof. Silvia Brunelli or Prof. Angelo A. Manfredi, School of Medicine and Surgery, University of Milano Bicocca, via Cadore 48, 20900, Monza, Italy (S.B.) or IRCCS San Raffaele Scientific Institute, via Olgettina 48, 20132 Milan, Italy (A.A.M.). E-mail addresses: silvia.brunelli@unimib.it (S.B.) or manfredi.angelo@hsr.it (A.A.M.)

The online version of this article contains supplemental material.

Abbreviations used in this article: Cll, clodronate; Col-1, collagen 1; EdC, endothelial-derived cell; EndoMT, endothelial-to-mesenchymal transition; EYFP, enhanced yellow fluorescent protein; FW, forward; IF, immunofluorescence; PAI-1, plasminogen activator inhibitor-1; pEC, primary endothelial cell; rm, recombinant mouse; REV, reverse; SSc, systemic sclerosis.

in tissues of SSc patients might be compatible with a role of macrophages in the regulation of EndoMT. In this study, we relied on an ad hoc in vivo genetic endothelial lineage tracing model to unequivocally demonstrate the contribution of EndoMT to the bleomycin-induced fibrosis of the lung and to verify if signals in the blood of patients with SSc or released in vitro and in vivo by macrophages influence the process.

Materials and Methods

Animals

Mice were housed in the specific pathogen-free facility at San Raffaele Scientific Institute and treated with the approval of the Institutional Animal Care and Use Committee (IACUC 489, 663). Cdh5-CRE^{ERT2} (25) and R26R–enhanced yellow fluorescent protein (EYFP) (26) mice were bred to yield heterozygous siblings and genotyped as in (25). Cre recombination was induced in Cdh5-CreERT2::R26R-EYFP mice at postnatal days 6–8 with three s.c. injections of tamoxifen (250 μg/mouse; Sigma-Aldrich, St. Louis).

Fibrosis

Six-week-old mice (three to four per group) were treated daily for 4 wk with s.c. injection of bleomycin (0.1 mg/mouse; Bleoprim, Sanofi, France) or PBS in the intrascapular region (27).

Phagocytes targeting

Mice were injected i.p. with liposomes containing either clodronate (Cll; 1.8 mg/mouse) or PBS (Sham) (http://www.clodronateliposomes.org/ashwindigital.asp?docid=26). The treatment was performed together with bleomycin injection and repeated every 2 d thereafter.

Immunofluorescence

Frozen sections of lung and kidney were fixed with 4% paraformaldehyde, permeabilized with PBS containing Triton (0.2%) and BSA (1%), and blocked with PBS containing serum (10%) and BSA (1%). Preblocked frozen sections were challenged, where indicated, with the following Abs: rat anti-mouse CD31 (1:2; kind gift from Elisabetta Dejana, Milan, Italy); rat anti-mouse VE-Cadherin (VE-Cad) (1:50; BD Pharmingen, NJ); rabbit anti-mouse collagen 1 (Col-1) (1:200; Abcam, Cambridge, U.K.); goat anti–α-SMA (1:200; Abcam); chicken anti-mouse GFP (1:500; Abcam); rabbit anti-mouse F4/80 (1:200; Bio-Rad, Kidlington, U.K.); rat anti-mouse CD163 (1:200; Santa Cruz Biotechnology, Dallas, TX) Abs. Appropriate Alexa Fluor (Alexa 488, Alexa 546, or Alexa 633)–conjugated Abs (1:500; Invitrogen) were used as second-step reagents. Images were acquired on a Zeiss LSM 710 (Zeiss, Oberkochen, Germany) and analyzed by ZEN 2009 software (Zeiss). Intensity and colocalization signals were quantified by ImageJ software.

Histochemistry

Serial lung or kidney sections were stained with Sirius Red (Sigma-Aldrich) per standard procedures, and pictures were acquired by Zeiss Imager 2 (Zeiss). To quantify fibrosis, pictures were analyzed using the batch mode of the ImageJ versus1.49 macro. Color thresholding algorithm used by this macro is based on an algorithm written by G. Landini (version v1.8) (http://www.mecourse.com/landinig/software/software.html).

Patients and controls

Venous blood was drawn into vacutainer tubes using a clot activator tube. Samples were incubated in an upright position at room temperature for 30–45 min to allow clotting and centrifuged for 15 min at 500 × *g*. Serum was carefully aspirated, aliquoted, and stored at −80°C. Blood was collected from 18 consecutive patients with SSc seen in October 2015 and five age- and sex-matched healthy volunteers after having signed written informed consent. The Ethical Committee of the San Raffaele Scientific Institute approved the serum biobanking (Autoimmuno-mol study). Patients were required to satisfy the 2013 ACR/EULAR Criteria for SSc (28). Exclusion criteria included cancer, concurrent acute or chronic infective condition, atrial fibrillation, moderate/severe chronic renal failure (glomerular filtration rate <60 ml/min), liver cirrhosis (Child–Pugh score B or C), and satisfaction of classification criteria for any other autoimmune disease. An exhaustive clinical and laboratory assessment was performed in accordance to the EULAR recommendations. Patients were characterized for skin involvement (limited cutaneous versus diffuse cutaneous SSc and modified Rodnan skin score, digital ulcers at the time of venipuncture). Patients were screened for pulmonary arterial hypertension by echocardiography and lung-function test. Lung fibrosis was defined by chest computed tomography (thickening of interlobular septa, traction bronchiectasis, honeycombing) or by lung-function tests (presence of a restrictive pattern not otherwise explained).

Flow cytometry

To isolate EdCs from Cdh5-CreERT2::R26R-EYFP, lung was minced and dissociated with Collagenase of *Clostridium histolyticum* (1.5 mg/ml; Roche, Basel, Switzerland) and Dispase (2.5 mg/ml; Life Technologies, Thermo Fisher Scientific, Waltham, MA) at 37 °C for 15 min (2 cycles). The resulting suspension was filtered (40–70 μM) and cells were resuspended in DMEM with 20% FBS, 20 mM HEPES, and 2 mM EDTA or with PBS with 2% FBS and 2 mM EDTA. Sorting of EYFP$^+$ cells was performed on the MoFLo XDP system (Beckman Coulter, Brea, CA). Where indicated, during EYFP$^+$ sorting, a double-staining was performed with anti-mouse CD31-allophycocyanin (eBioscience, Thermo Fisher Scientific) and anti-mouse VE-Cad-PE (BioLegend, San Diego, CA) Abs. Data were analyzed using FlowJo software (TreeStar, Ashland, OR). Flow cytometry was performed using anti-mouse F4/80-allophycocyanin (eBioscience, Thermo Fisher Scientific) and anti-mouse CD11b-PE-Cy7 (BD Pharmingen) with the BD FACS Accuri system (BD, Franklin Lakes, NJ). Data were analyzed by FACSDIVA software (BD).

Cell culture

Mouse primary endothelial cells (pECs) (29) were grown in high-glucose DMEM (Lonza) supplemented with FBS (10% Lonza; Basel, Switzerland) and vascular endothelial growth factor (mouse-VEGF 10 ng/ml; PeproTech, Rocky Hill, NJ). Where indicated, pECs were treated for 5 d with high-glucose DMEM supplemented with FBS 2% and enriched with SSc heat-inactivated serum or with FBS as control (20%; 1:5 dilution) or TGF- β1 (10 ng/ml; PeproTech). Where mentioned, SSc heat-inactivated serum was also used at 10% (1:10 dilution) or 2% (1:50 dilution).

Sera IgG depletion

SSc Scl70+ heat-inactivated sera were depleted of IgG with PureProteome Albumin/IgG Depletion Kit (Millipore Merck, Darmstadt, Germany) according to manufacturer's recommendations. Sera were diluted 1:2 × 10^6 to measure IgG level with human IgG ELISA kit (Abcam) to verify IgG depletion. To evaluate effects of IgG-depleted sera, pECs were treated for 48 h with high-glucose DMEM supplemented with FBS 2% and enriched with IgG depleted or undepleted SSc heat-inactivated sera (1:5 dilution) or with FBS as control (20%; 1:5 dilution).

Tube formation assay

pECs were propagated for 5 d in the presence of SSc serum or FBS and plated on μ-Slide Angiogenesis (Ibidi, Munich, Germany) per manufacturer recommendations. After polymerization of Matrigel (Matrigel Growth Factor Reduced, 10 μl/well; Corning, NY) cells (30,000 per well) were suspended in minimal medium and plated in triplicate per each experimental condition. Tube formation was followed for 6 h, and microphotographs were taken every hour. The tube formation analysis was performed using the WimTube online software (https://www.wimasis.com/en/products/13/WimTube).

Migration assay

pECs were plated on 24-well plates and propagated for 5 d in the presence of SSc serum or FBS. A scratch was performed on the pECs monolayer with a p200 tip, and phase contrast microphotographs for each well was taken every 3 h for 24 h. ImageJ was used to analyze the width of the scratch.

Isolation and polarization of mouse macrophages

Bone marrow cells from flushed femurs and tibias of C57BL/6 female mice were propagated for 5 d in α-modified Eagle's medium (α-MEM) (Life Technologies/Invitrogen, Carlsbad, CA) containing FBS (10%) in presence of recombinant mouse (rm) M-CSF (100 ng/ml) (30). Cells were propagated for two additional days in the presence of rm–IFN-γ (50 ng/ml) to generate M1 cells, or for four additional days with rm–M-CSF (10 ng/ml) and rm–IL-4 (10 ng/ml) or rm–IL-10 (10 ng/ml) for M2a and M2c, respectively (all cytokines are from PeproTech).

Macrophage-pECs coculture assays

Macrophage conditioned media were prepared by seeding undifferentiated macrophages in six wells plates (1 × 10^6/ml). After polarization, cells were washed twice with PBS. α-MEM containing FBS (2%) was added for 24 h. Supernatants were collected, centrifuged at 13,000 × *g* for 5 min, recovered,

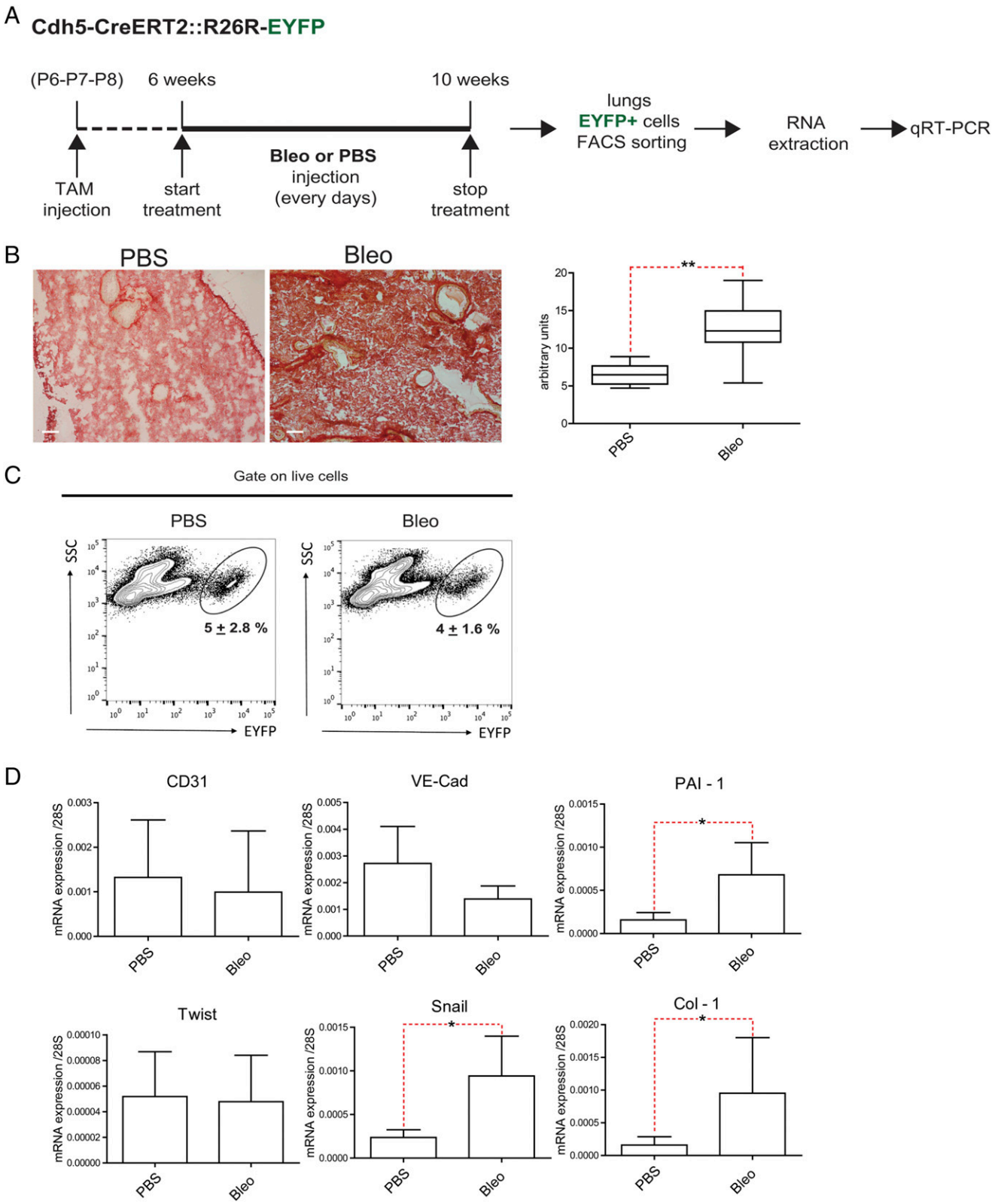

FIGURE 1. s.c. bleomycin (Bleo) elicits fibrosis and EndoMT in the lung of Cdh5-CreER^{T2}::R26R-EYFP transgenic mice. (**A**) Experimental setting used to induce systemic inflammation and fibrosis with Bleo in Cdh5-CreER^{T2}::R26R-EYFP mice. CRE activation was achieved by tamoxifen (TAM) injection at postnatal days 6, 7, 8 (P6-P7-P8). Six-week-old Cdh5-CreER^{T2}::R26R-EYFP mice were treated with daily s.c. injection of PBS or of Bleo for 4 wk. (**B**) Left, Representative image of lung sections of Bleo- or PBS-treated Cdh5-CreER^{T2}::R26R-EYFP mice. Sirius Red was used to evaluate fibrosis and collagen accumulation. Scale bar, 100 μm. Graph on the right represents the quantification of Sirius Red staining obtained by ImageJ analysis expressed as arbitrary units. Data are expressed as mean ± SEM $^{**}p < 0.005$. ($n = 3$). (**C**) Gating strategy employed to isolate EYFP^{+} cells from the lung of PBS- or Bleo-treated mice. Numbers indicate the percentage of EYFP^{+} cells. Data are represented as mean ± SEM ($n = 4$). (**D**) Quantitative RT-PCR analysis of EYFP^{+} cells freshly sorted from the lung of Cdh5-CreER^{T2}::R26R-EYFP mice after PBS or Bleo treatment using primers specific for CD31,VE-Cad, PAI-1, Twist1, Snail1, and Col-1. Gene expression data are relative to 28S. Data are expressed as mean ± SEM $^{*}p < 0.05$. ($n = 4$).

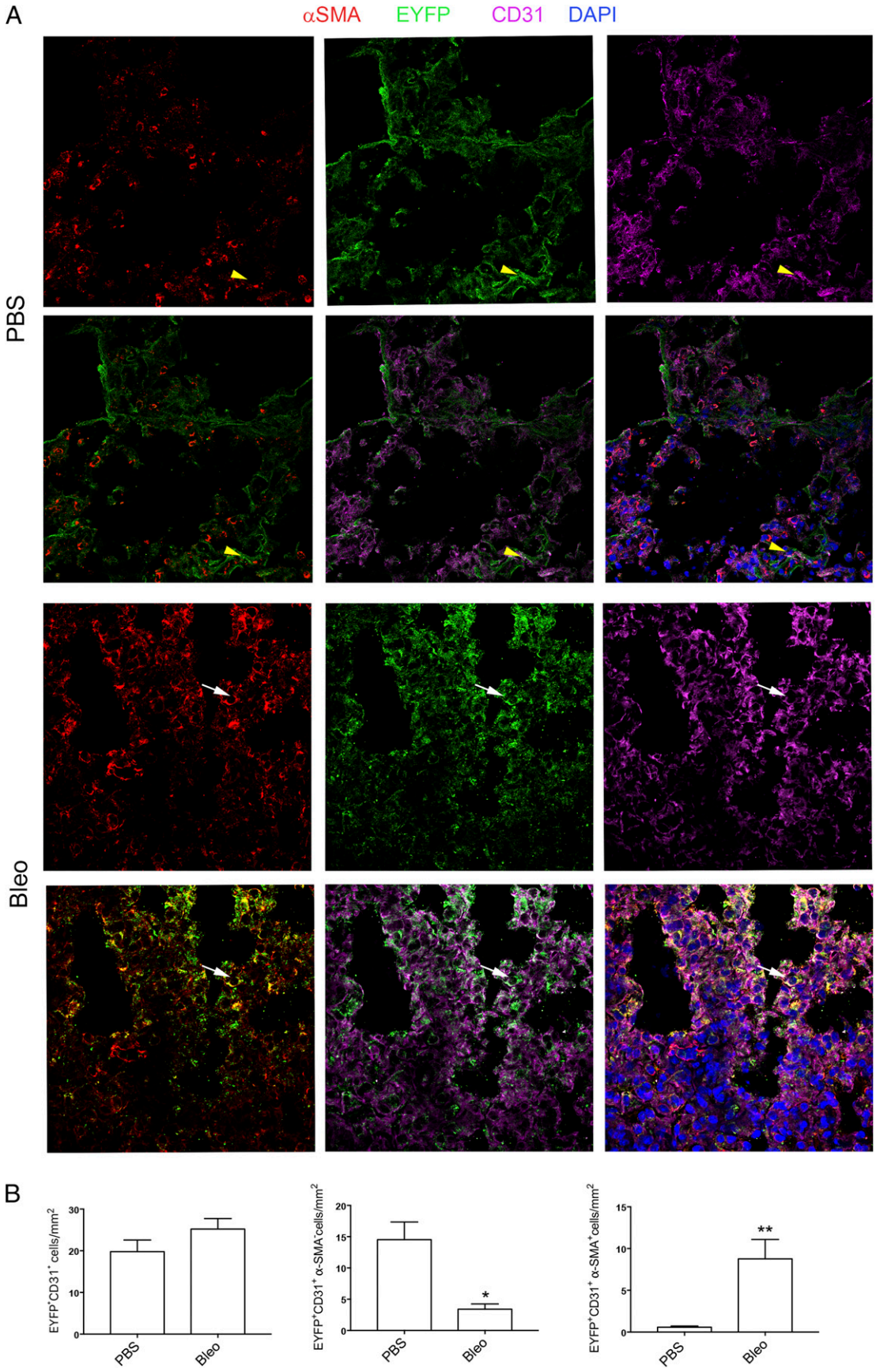

FIGURE 2. s.c. bleomycin (Bleo) elicits EndoMT in the lung of Cdh5-CreER^{T2}::R26R-EYFP transgenic mice. (**A**) Representative IF staining using Abs specific for CD31 (endothelium; violet), α-SMA (myofibroblasts; red), and EYFP$^+$ (endothelial cells and EdCs; green) on lung section of PBS- or of Bleo-treated Cdh5-CreER^{T2}::R26R-EYFP mice. Nuclei are counterstained with DAPI (blue). White arrows: EYFP$^+$α-CD31$^+$ SMA$^+$ cells, yellow arrowheads: EYFP$^+$ CD31$^+$ cells. Scale bar, 50 μm. (**B**) Quantification of EYFP$^+$ CD31$^+$α-SMA$^-$ or α-SMA$^+$ in lungs of PBS- or Bleo-treated mice. Data are expressed as mean ± SEM (n = 4 mice per group). *$p < 0.05$, **$p < 0.01$.

and stored at −80°C, and when indicated, added upon thawing to pECs for 24 h.

Quantitative RT-PCR analysis

Total RNA from EdCs or pECs was isolated using ReliaPrep RNA Cell Miniprep System (Z6011; Promega, Milan, Italy). Reverse transcription was performed on total RNA (1 μg) using the MultiScribe reverse transcriptase (Applied Biosystems, Warrington, U.K.). Analysis was carried on a MX 3000 Real-Time PCR detection system (Stratagene, La Jolla, CA). cDNAs were amplified using Brilliant Quantitative PCR Core Reagent Kit mix and SYBR Green 0.333 (Applied Biosystems, Cleveland, OH). Primer sequences are listed in below. Cycle threshold (C_T) values >45 were considered negative. Data points were analyzed in triplicate. Quantification was performed using the comparative C_T method. Internal controls: 28S.

Primers sequences. Primer sequences were as follows. CD31 forward (FW): 5′-AGGGGACCAGCTGCACATTAGG-3′; CD31 reverse (REV): 5′-AGGCCGCTTCTCTTGACCACTT-3′; VE-Cad FW: 5′-GTACAGCATCATGCAGGGCG-3′; VE-Cad REV: 5′-ATTCGTATCGGATAGTGGGG-3′; CD34 FW: 5′-TTGACTTCTGCAACCACGGA-3′; CD34 REV: 5′-TAGATGGCAGGCTGGACTTC-3′; CD73 FW: 5′-CAAATCCCACACAACCACTG-3′; CD73 REV: 5′-TGCTCACTTGGTCACAGGAC-3′;PAI-1 FW: 5′-TCCTCCACAGCCTTTGTCAT-3′; PAI-1 REV: 5′-ACATCTCCACTTTCGTCCCA-3′; Twist FW: 5′-GGACAAGCTGAGCAAGATTCA-3′; Twist REV: 5′-CGGAGAAGGCGTAGCTGAG-3′; Snail1 FW: 5′-CACACGCTGCCTTGTGTCT-3′; Snail1 REV: 5′-GGTCAGCAAAAGCACGGTT-3′; Col-1 FW: 5′-GGTATGCTTGATCTGTATCTGC-3′; Col-1 REV: 5′-AGTCCAGTTCTTCATTGCATT-3′; α-Sma FW: 5′-TCACCATTGGAAACGAACG-3′; α-Sma REV: 5′-ATAGGTGGTTTCGTGGATGC-3′; 28S FW: 5′-AAACTCTGGTGGAGGTCCGT-3′; 28S REV: 5′-CTTACCAAAAGTGGCCCACTA-3′.

Statistical analysis

Data were analyzed with Microsoft Excel 14.1.0 and GraphPad Prism 6 and plotted as mean ± SEM. To evaluate statistical significance unpaired two-tailed Student *t* tests or nonparametric Mann–Whitney were used assuming equal variance.

Results

Bleomycin treatment induce EndoMT in lung endothelial precursors

To explore the fate of endothelial progenitors and EdC in a mouse model of SSc, we took advantage of a genetic lineage tracing model. A tamoxifen-inducible form of Cre recombinase (CRE-ER^{T2}) was placed under the control of the endothelial-specific gene *VE-Cad* regulatory sequences, Cdh5-$CreER^{T2}$ (25). Mice were crossed with the reporter mice R26R-EYFP (26). Cre recombination was induced in double transgenic mice at stages P6–P8 to irreversibly label postnatal VE-Cad–expressing EdCs. This mouse model guarantees very high efficiency and specificity of the original labeling of endovascular progenitors and mature endothelial cells (21, 31); around 95% of the $EYFP^+$ cells express the endothelial marker CD31, and it is possible to follow the fate of EdC even after downregulation of endothelial markers (21) (Supplemental Fig. 1A, 1B).

To model SSc-associated fibrosis, we injected Cdh5-$CreER^{T2}$::R26R-EYFP mice with s.c. bleomycin every day for 4 wk (Fig. 1A). The advantage of s.c. bleomycin is the induction of lung fibrosis, inflammation, and lesion at subpleural and perivascular level, as a consequence of a systemic process and not as the result of a local injury. The systemic event induced by the s.c. treatment moreover allows us to study the modulation of the elicited fibrotic events in other tissues involved in the natural history of SSc (32–35). Lung sections revealed extensive collagen accumulation as assessed by Sirius Red histochemical staining (Fig. 1B). We retrieved by cell-sorting $EYFP^+$ EdCs from the lung of bleomycin- and sham-treated mice. The yield was similar, suggesting that bleomycin did not per se deplete EdCs (Fig. 1C). We verified if endothelial cells in the fibrotic lung expressed EndoMT-related genes: the basic helix-loop-helix transcription factor Twist, the zinc finger transcription factors Snail1, a member of the serine protease inhibitor family, plasminogen activator inhibitor-1 (PAI-1) and Col-1 (15). $EYFP^+$ EdCs of bleomycin-treated mice expressed significantly higher levels of Snail1, PAI-1, and Col-1 but not of Twist (Fig. 1D). They did not significantly downregulate the expression of CD31 and VE-Cadherin (Fig. 1D). We also show by IF that $EYFP^+$ EdCs expressing α-SMA were more numerous in the lung of bleomycin-treated than of PBS-treated mice (Fig. 2A, 2B, Supplemental Fig. 2A, 2B). Conversely, we observed a decrease of $EYFP^+CD31^+\alpha\text{-}SMA^-$ cells (Fig. 2A, 2B). These results confirm that EndoMT is occurring and that we may have different endothelial populations, having different tendency to undergo EndoMT, and/or that we may witness both complete and intermediate transition.

Soluble signals in the sera of SSc patients prompt EndoMT in vitro

The serum of SSc patients contains soluble factors that exacerbate systemic vasculopathy and fibrosis, potentially by modulating EndoMT (20, 36–38). We took advantage of pEC that retains plasticity in vitro and in vivo after transplantation (29). pECs underwent EndoMT when challenged with TGF-β1, acquiring elongated and fibroblastic shapes and expressing the mesenchymal associated genes PAI-1, Twist, and Snail1 [Supplemental Fig. 1C, 1D; see also (39)]. pECs were challenged with individual sera [diluted 1:5, as in (20)] from SSc patients or healthy donors for 5 d. Clinical features of patients are shown in Table I. Anti-topoisomerase 1 (anti-Scl70) Abs are known to associate in SSc patients diffuse cutaneous fibrosis, more frequent involvement of internal organ, and worse prognosis (2, 40). Accordingly, in our study, we used the presence anti-Scl70 Abs to identify patients with a higher probability of a severe clinical course and of developing more extensive fibrosis of the skin and organ fibrosis. All SSc sera influenced pEC morphology (from a cobblestone-like to a fibroblastic appearance), mimicking the effect of the cytokine, TGF-β1 (Fig. 3A, Supplemental Fig. 1C), but we never observed signs of pEC activation, damage, or death (data not shown). All SSc sera induced the upregulation in pECs of the expression of

Table I. Demographic and clinical characteristics of the 18 patients with SSc used for collection of serum samples

Characteristics	Value
SSc patients, *n*	18
Mean age (range), y	52.5 (26–76)
Gender	Female
Mean disease duration (range), y	9 (1–23)[a]
Antinuclear Abs, *n*	18
Anti-topoisomerase I Abs (anti-Scl70), *n*	12[b]
Lung fibrosis, *n*	1
Early lung fibrosis, *n*	1
Heart failure, *n*	1
Gastrointestinal involvement, *n*	1
Active inflammatory articular/ musculoskeletal features, *n*	3
Anti-centromere Abs, *n*	5
Mean modified Rodnan skin score (range)	9 (0–45)[c]
Mean anti-$Scl70^-$ patients	4.8
Mean anti-$Scl70^+$ patients	8.9
Limited SSc, *n*	13
Diffused SSc, *n*	5
Pulmonary arterial hypertension, *n*	0
Renal crisis, *n*	0
Erythrocyte sedimentation rate, mean (range)	13.9 (7–31)[d]
C-reactive protein, mean (range)	2.8 (0.8–5.9)[d]

[a]Disease duration was calculated since the first non-Raynaud's symptom of SSc.
[b]No anti-Scl70 patients had these symptoms.
[c]Data not available for four patients.
[d]Data not available for two patients.

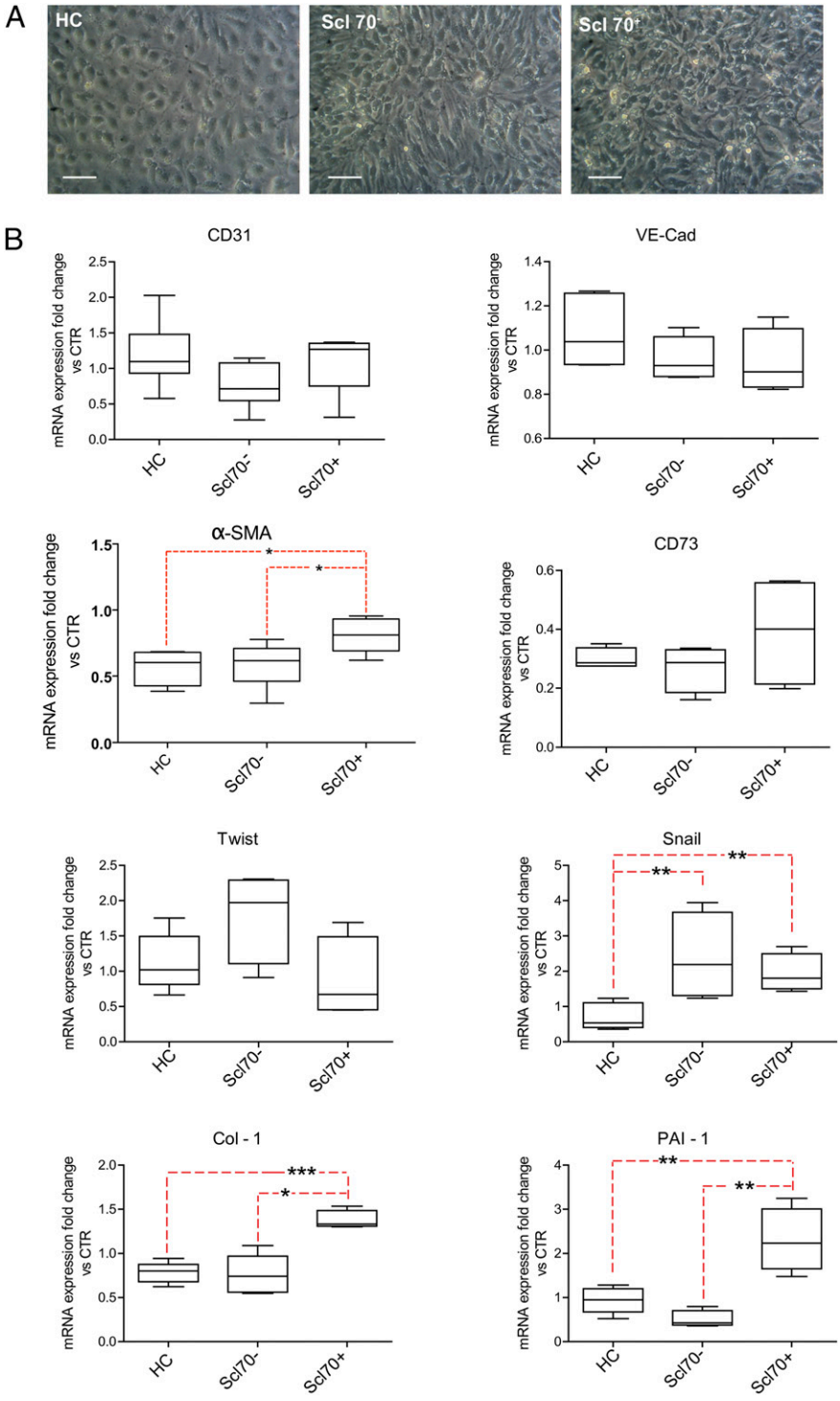

FIGURE 3. Sera from SSc patients induce EndoMT in pECs in vitro. (**A**) Representative phase contrast microphotographs of pECs after the treatment with serum collected from healthy controls (HC), from anti-Scl70–negative SSc patients (Scl 70^{-}), or from anti-Scl70–positive SSc patients (Scl 70^{+}). Scale bar, 200 μm. (**B**) Quantitative RT-PCR analysis of pECs challenged with SSc patient sera, stratified by presence of anti-Scl70 Abs, using primers specific for CD31, VE-Cad, CD73, Twist1, Snail1, α-Sma, Col-1, and PAI-1. Gene expression data are relative to 28S. Values represent the fold change with respect to treatment with 20% FBS. Data are expressed as mean ± SEM ($n = 4$). $*p < 0.05$, $**p < 0.005$, $***p < 0.0005$.

Snail1 (Fig. 3B). Only sera from Scl70^{+} patients scientifically upregulated the expression of the EndoMT/mesenchymal marker PAI-1, Col1, and α-SMA (Fig. 3B). EndoMT-inducing ability of Scl70^{+} sera was inversely proportional to sera dilution (Supplemental Fig. 3A) but was not affected by IgG depletion (Supplemental Fig. 3B). Control sera did not influence the expression of any EndoMT/mesenchymal markers, and no sera had effect on the expression of endothelial markers CD31 and VE-Cad or the mesenchymal stem cells marker CD73 (Fig. 3B).

The tube formation assay measures the ability of endothelial cells to differentiate and to form tube-like structures (41). Sera from Scl70^{+} patients abrogated the ability of pEC to yield vasculogenesis, as assessed by the area covered by neoformed tubes, the total length of endothelial tubes, the number of branching points, and loops reflecting vessels (Fig. 4A, 4B). Moreover, pECs exposed to sera of Scl70^{+} patients migrated and invaded the wound significantly more, as assessed in an in vitro wound healing scratch assay (Fig. 4C, 4D).

Macrophages protect from lung fibrosis and EndoMT

We targeted macrophages by injecting liposomes containing Cll (or PBS) i.p. every 2 d in bleomycin-treated Cdh5-CreER^{T2}::R26R-EYFP mice (Supplemental Fig. 4A). Blood Cd11b^{+}F4/80^{+} cell counts were significantly reduced in Cll-versus sham-treated mice,

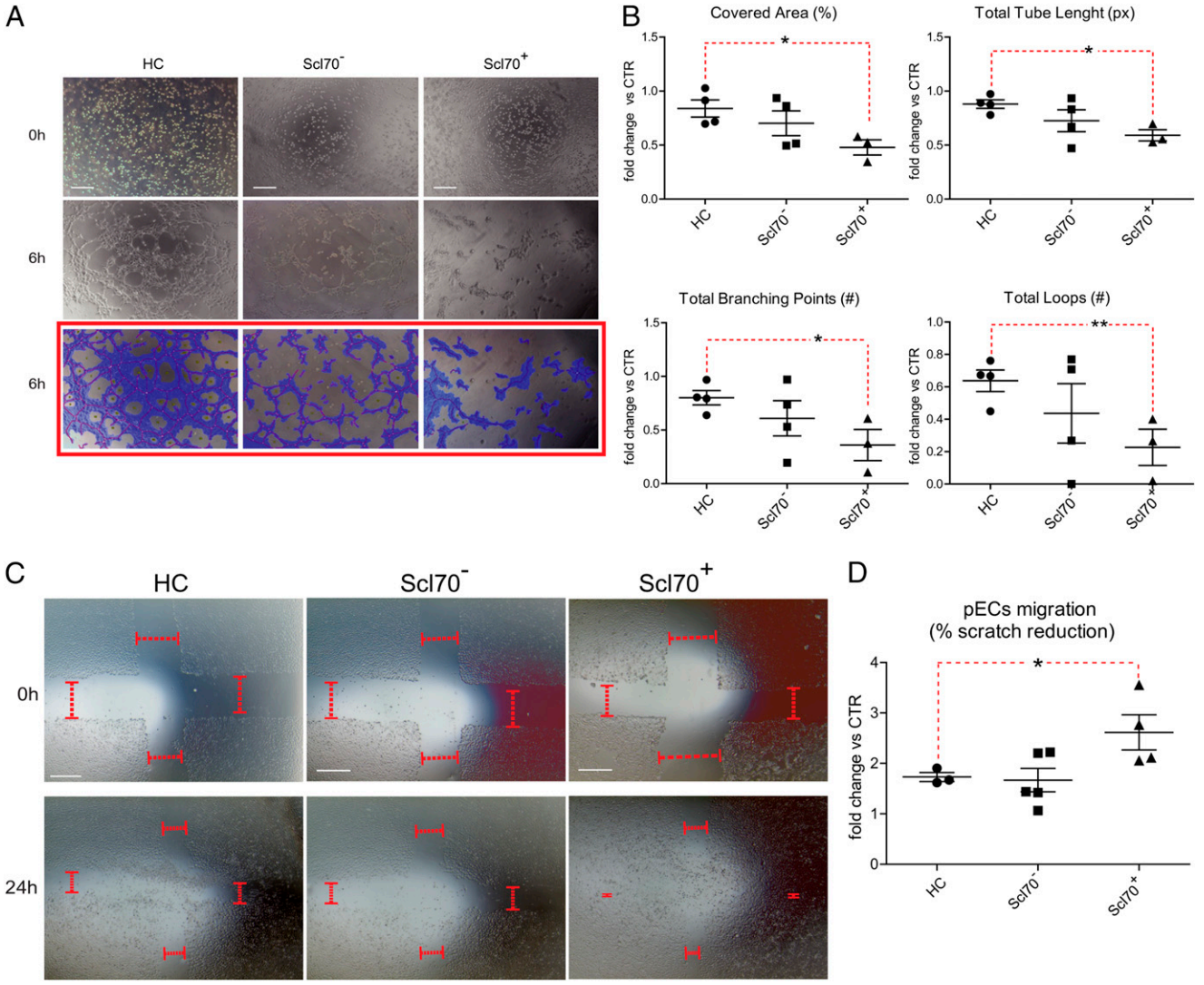

FIGURE 4. Sera from SSc patients influence angiogenic and migratory ability of pECs. (**A** and **B**) Tube formation assay of pECs pretreated with sera from healthy control donors (HC), Scl70$^-$, or Scl70$^+$patients. (A) Representative images of phase contrast microphotographs of pretreated pECs at time 0 (top panels) and 6 h (center panels) after the beginning of the tube formation assays. In the bottom panels, images of the middle panels are shown after the analysis with the Wimasis WimTube Solution software. Scale bar, 200 μm. (B) Graphs summarizing the quantification measured 6 h after the beginning of the assay of percentage (%) of the area covered by tubes, total tube length (px, pixels), total branching points (#, number), total loops (#, number). Values represent the fold change respect to treatment with 20%FBS (CTR). Data are expressed as mean ± SEM ($n = 3$). *$p < 0.05$, **$p < 0.005$. (**C** and **D**) Scratch assay on pECs pretreated with sera from healthy controls (HC), Scl70$^-$, or Scl70$^+$ patients. (C) Representative image of phase contrast microphotographs of pECs at time 0 and 24 h. Red dotted lines indicate the edge of the wound. Scale bar, 200 μm. (D) Quantification of the reduction of the wound size after 24 h (% scratch reduction), expressed as fold change respect to treatment with 20% FBS (CTR). Data are expressed as mean ± SEM ($n = 3$). *$p < 0.05$, **$p < 0.005$.

indicating that phagocyte targeting was effective (Supplemental Fig. 4B). CD163$^+$F4/80$^+$ alternatively activated macrophages were preferentially targeted in solid organs, including the lung, assessed by IF (Fig. 5A, 5B, Supplemental Fig. 4C). Sirius Red histochemistry showed increased collagen accumulation in bleomycin–Cll with respect to bleomycin–sham-treated mice (Fig. 5C, Supplemental Fig. 4D). In agreement, we observed more EdCs expressing EndoMT markers, such as Col-1 (Fig. 6A, 6B).

Macrophage depletion per se did not affect the number of EdC that could be isolated from the lung after bleomycin treatment (Fig. 5D) or the expression of endothelial markers (Fig. 5E, 5F), but in these cells, expression of the EndoMT associated genes, Snail1, and Col1 were selectively increased after fibrosis induction and macrophage depletion (Fig. 5F). Thus, if macrophages fail to prevent EdC transition toward a mesenchymal phenotype, fibrosis was enhanced. Interestingly, signals released by macrophages propagated with IL-10, which prompts CD163 expression and alternative activation, regulated Snail1 and Col-1 expression in pEC treated with Scl70$^+$ sera (Table II). Again, expression of endothelial markers was not affected.

Discussion

Persistent inflammation in SSc eventually causes obliteration of the microvasculature and disruption of the organ architecture, owing to accumulation of fibrotic material. Microenvironmental signals influence vasculopathy and fibrosis, jeopardizing the ability of tissues to face hypoxia, to initiate effective vasculogenesis, and eventually to heal (5, 42). Macrophages are both a player and a target in SSc (43). They play an apical role in the innate response to inflammatory stimuli (44, 45). A "useful simplification" of what is in vivo a broad and partially overlapping array of differentiating populations suggests that activated macrophages yield M1

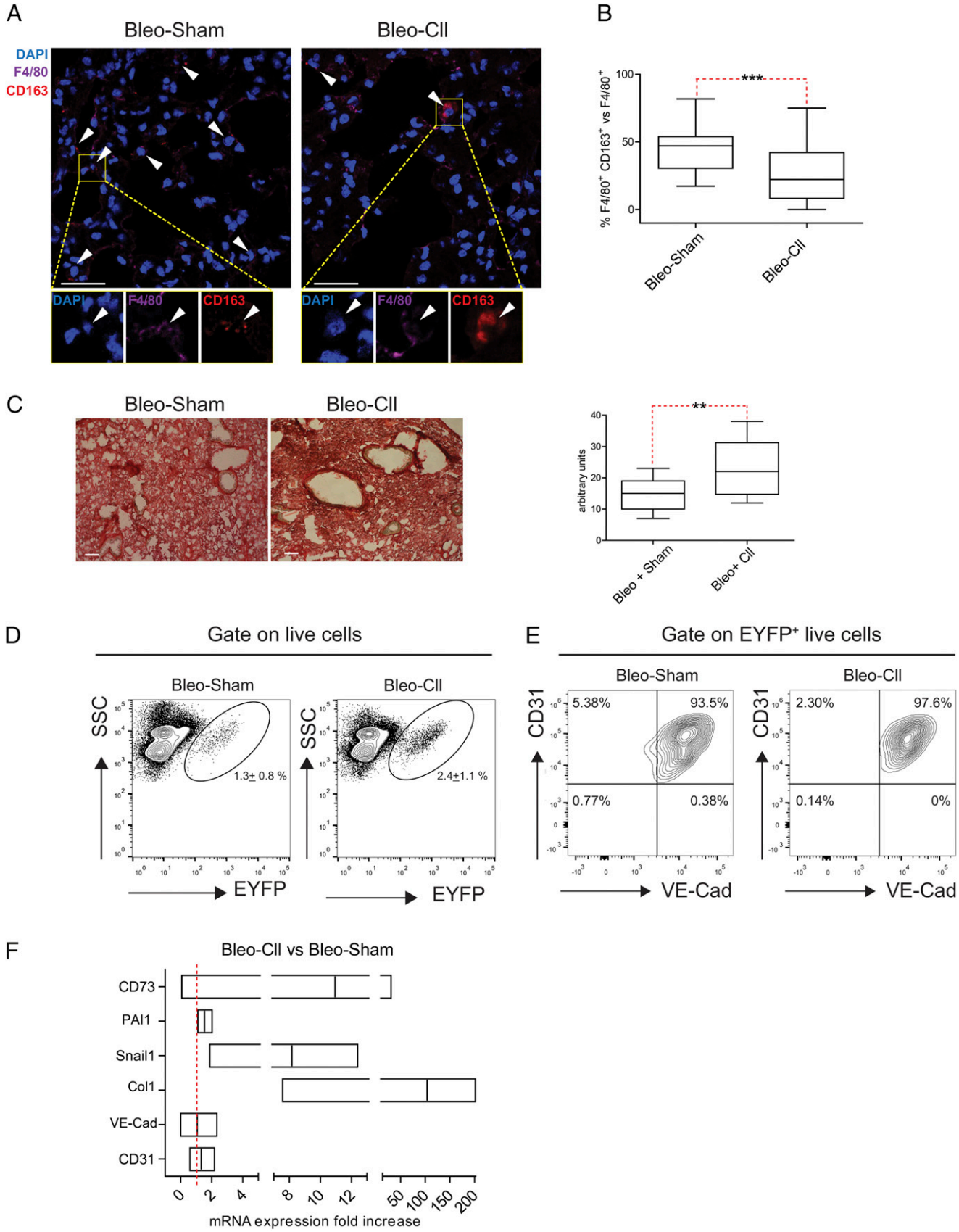

FIGURE 5. Macrophages mice limit lung fibrosis in bleomycin (Bleo)-treated Cdh5-CreER^{T2}:: R26R-EYFP transgenic and EndoMT. (**A**) Representative IF after staining with Abs specific for F4/80 (violet) and for CD163 (red), of lung sections from Bleo-treated Cdh5-CreER^{T2}::R26R-EYFP mice, injected with Cll or (Sham) containing liposomes (Bleo-Cll and Bleo-Sham, respectively). Nuclei are counterstained with DAPI (blue). White arrowheads: double positive F4/80^{+}CD163^{+} cells. Scale bar, 100 μm. (**B**) Graph representing the percentage of the F4/80^{+}CD163^{+}double positive cells respect to the total F4/80^{+} in the lungs of Bleo-treated Cdh5-CreER^{T2}::R26R-EYFP mice (percentage F4/80^{+}CD163^{+} versus F4/80^{+}), injected with either Cll or Sham liposomes. Data are expressed as mean ± SEM (n = 3 mice per group). ***$p < 0.0005$ (**C**) Representative images of lung *(Figure legend continues)*

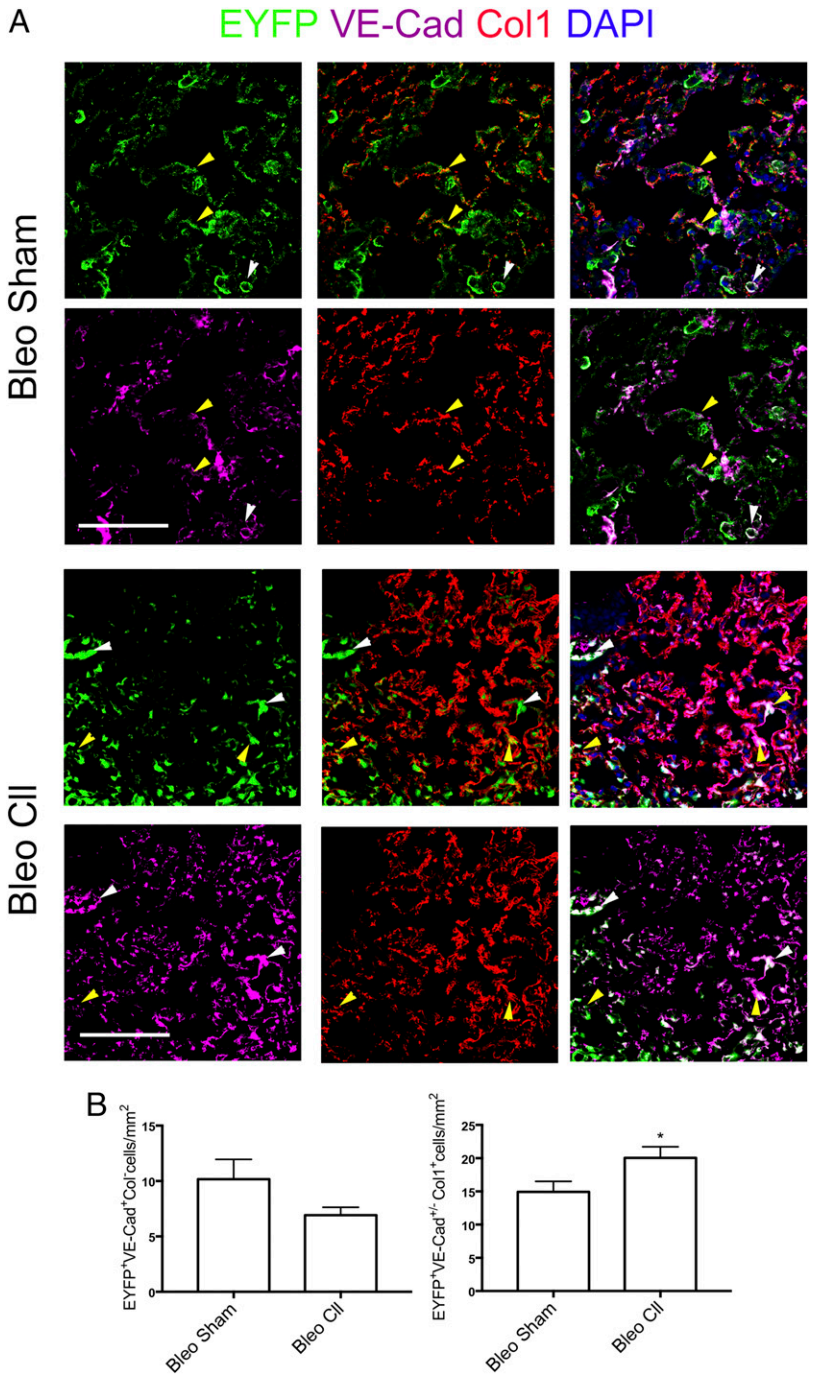

FIGURE 6. Macrophages in bleomycin (Bleo)-treated Cdh5-CreER^{T2}:: R26R-EYFP transgenic mice hamper EndoMT in vivo. (**A**) Representative IF staining using Abs specific for VE-Cad (endothelium; violet), Col-1 (myofibroblasts; red), and EYFP (endothelial cells and EdCs; green) on lung sections collected from Bleo-sham or Bleo-Cll treated Cdh5-CreERT2::R26R-EYFP mice. Nuclei are counterstained with DAPI (blue). Yellow arrowheads: representative EYFP$^+$Col-1$^+$ positive cells. White arrowheads: representative of EYFP$^+$VE-Cad$^+$Col-1$^-$ positive cells. Scale bar, 100 μm. (**B**) Quantification of EYFP$^+$VE-Cad$^+$Col$^-$ or EYFP$^+$VE-Cad$^{+/-}$Col$^+$ cells in section of Bleo-Sham or Bleo-Cll treated mice) Data are expressed as mean ± SEM (n = 3 mice per groups). *$p < 0.05$.

("classically activated") and M2 ("alternatively activated") cells (45). M1 macrophages are mainly in charge of the response against pathogens and M2 macrophages of later phases of inflammation, promoting angiogenesis, clearance of dying cells and debris, and tissue regeneration and adaptation (45, 46). Alternatively activated macrophages prompt precursor differentiation to myofibroblasts, which oversee to the production of the matrix for tissue regeneration. These macrophages dominate in tissues of patients with rheumatic diseases, including SSc, and might favor fibrosis (22, 23, 47). However, macrophage role might be more complex than

sections of Bleo-treated Cdh5-CreER^{T2}::R26R-EYFP mice, injected with Cll- or sham-containing liposomes (Bleo-Cll and Bleo-Sham, respectively), stained with Sirius Red. Scale bar, 50 μm. Graph on the bottom represents the quantification (expressed as arbitrary units) of Sirius Red staining obtained by ImageJ analysis. Data are expressed as mean ± SEM (n = 3 mice per group). **$p < 0.005$. (**D**) Gating strategy employed to isolate EYFP$^+$ cells from the lungs of Bleo-treated Cdh5-CreER^{T2}::R26R-EYFP mice, injected with Cll- or sham-containing liposomes (Bleo-Cll and Bleo-Sham, respectively). Numbers indicate the percentage (%) of EYFP$^+$ cells. Data are represented as mean ± SEM (n = 3). (**E**) Plot representing the percentage of VE-Cad$^+$ and CD31$^+$ in the isolated EYFP$^+$ population in (D). (**F**) Quantitative RT-PCR analysis of EYFP$^+$ cells freshly sorted from Bleo-treated Cdh5-CreER^{T2}::R26R-EYFP mice, injected with Cll- or sham-containing liposomes (Bleo-Cll and Bleo-Sham, respectively) using primers for CD73, PAI-1, Snail1, Col-1, VE-Cad, or CD31. Gene expression data are relative to 28S. Data are expressed as fold change (from minimum to maximum value) of Cll treated mice versus Sham (n = 3).

Table II. Conditioned medium from IL-10–polarized alternatively activated macrophages counteracts increased expression of Snail and Col-1 EndoMT markers, induced by SSc Scl70$^+$ sera

Fold Change (Mean ± SEM)	Sera	Sera + Conditioned Medium
CD31	1.05 ± 0.25	1.18 ± 0.25
VE-Cad	0.99 ± 0.06	0.91 ± 0.07
CD73	0.39 ± 0.09	0.24 ± 0.02
PAI-1	3.06 ± 1.09	3.78 ± 1.21
Snail1	1.98 ± 0.19	1.31 ± 0.23*
Col-1	2.39 ± 1.02	1.59 ± 0.79**

Quantitative RT-PCR analysis of endothelial (CD31 and VE-Cad), mesenchymal stem cell (CD73), and mesenchymal/myofibroblast (PAI-1, Snail1, and Col-1) markers on pECs after treatment with Scl70+ SSc sera for 5 d, and further grown 24 h without (Sera) or with conditioned media from in vitro IL-10–polarized macrophages. Gene expression data are relative to 28S. Values represent the fold change with respect to treatment with only 20% FBS (CTR) followed by 24 h culture without conditioned media. Data are expressed as mean ± SEM.

*$p < 0.05$, **$p < 0.01$ with respect to treatment with only Scl70$^+$ SSc serum (Sera) ($n = 6$).

anticipated because alternatively activated cells also play angiogenic and vascular protective roles in inflamed tissues (45, 46).

Endothelial cells are a target of the disease both in patients with SSc and in experimental models of fibrosis (17, 18). Little is known on their fate or, in particular, on whether they die in situ, move away, or locally differentiate toward myofibroblasts. EndoMT shapes tissue adaptation during development and repair/remodeling in the adult life (14, 15, 39, 48). It might contribute to the natural history of SSc (12, 20, 49). By means of endothelial-specific genetic lineage tracing mice (21, 50), we followed the fate of EdCs during fibrosis, focusing on the main tissue target of SSc, the lung. After fibrosis induction, several lung EdCs express α-SMA, a marker of activated myofibroblasts (15). Moreover, they express Snail1, a regulator of signaling downstream TGF-β, Notch, and BMP and direct target of hypoxia inducible factor 1α (HIF-α) (51), which represses the expression of endothelial markers while prompting the expression of α-SMA (52). They also express PAI-1, a mesenchymal and profibrotic marker, target of TGF-β, expressed in endothelial cells undergoing EndoMT (33, 53, 54), and the ECM protein associated with fibrosis Col-1 (15). Still, the total number of EdC appear not to change, as the expression of endothelial markers CD31 and VE-cadherin, suggesting that our fibrosis model correlates more with an endothelial cell alteration respect to an endothelial cell reduction. It has been reported that the Cdh5-CreER^{T2} lineage tracing mice label endothelial cells with different potency (50), therefore with different predisposition to undergo EndoMT (55). Partial EndoMT, with maintenance of endothelial markers expression, has been described to play a role in physiological/pathological angiogenesis (56). Dermal microvascular endothelial cells from the skin of SSc patients but not of controls express Snail (20). Moreover, immunohistochemical staining and study of transcripts and proteins of SSc lungs revealed the simultaneous expression of mesenchymal and endothelial molecules (57). Our results agree with these observations and formally prove that the EndoMT contributes to the endothelial defect in SSc. Nevertheless, single-cell transcriptomic analysis on EdC in the different condition will be required to determine the role of specific endothelial subpopulation in fibrosis development triggered by multiple signaling and SSc onset and progression.

Previous lineage tracing studies suggested that Tie2-expressing precursors yield myofibroblasts (49). Our results allow to exclude a contribution to EndoMT of Tie2-expressing hematopoietic progenitors, which comprise macrophages that favor angiogenesis in cancer, liver regeneration, myelofibrosis, and endometriosis (50, 58, 59). Signals in the blood are associated with SSc severity and tissue involvement (e.g., 20, 36–38). In our system SSc sera favor the expression of EndoMT genes in pEC, quenching their angiogenic ability while boosting motility and invasive properties. In particular, signals promoting EndoMT are more expressed in patients at higher risk of involvement of visceral organ (patients bearing the Anti-topoisomerase 1 Ab, Scl70), including lung fibrosis (28). Further characterization of the EndoMT inducing signals specifically present in the sera of Scl70$^+$ patients is warranted.

With all the limitations associated with animal models and the fact that bleomycin-induced fibrosis only partially reproduces SSc, we observed in the mouse that targeting of lung macrophages impacted both on fibrosis and EndoMT. Gene expression profiling of SSc tissues supports an alternative activation of lung resident macrophages (60). As expected in a disease characterized by persistent remodeling of tissues (22, 23, 60–62). Studies using anti–IL-6R Abs support the involvement of macrophage alternative activation in fibrosis and in the clinical outcome (62, 63). Our data suggest that among macrophages infiltrating tissues undergoing fibrosis, at least some support angiogenesis and vasculogenesis (64). IL-10, which selectively induces upregulation of the scavenger receptor, CD163 and influences the response to hypoxia, enhances the macrophage proangiogenetic ability (65). In agreement, CD163 macrophages in the lung of mice treated with bleomycin may play a nonredundant role in sustaining angiogenesis and counteracting EndoMT.

Current therapies for fibrosis in SSc are disappointing. An intense effort is being made to target the innate immune system and to restore the ability of tissues to face hypoxia, thus preventing fibrosis. The pivotal role of macrophage in orchestrating the response to sterile damage makes them a convincing target (62, 66). In this scenario, agents that selectively sustain macrophages to guard EndoMT might be valuable in the persistently hypoxic tissue of patients with SSc.

Acknowledgments

Flow cytometry experiments have been carried out in the FRACTAL Cytometry facility (San Raffaele Scientific Institute, Milano, Italy). We thank Fabio Manenti for technical help with the macrophage polarization in vitro.

Disclosures

The authors have no financial conflicts of interest.

References

1. Gabrielli, A., E. V. Avvedimento, and T. Krieg. 2009. Scleroderma. *N. Engl. J. Med.* 360: 1989–2003.
2. Denton, C. P., and D. Khanna. 2017. Systemic sclerosis. *Lancet* 390: 1685–1699.
3. Matucci-Cerinic, M., B. Kahaleh, and F. M. Wigley. 2013. Review: evidence that systemic sclerosis is a vascular disease. *Arthritis Rheum.* 65: 1953–1962.
4. Wigley, F. M. 2009. Vascular disease in scleroderma. *Clin. Rev. Allergy Immunol.* 36: 150–175.
5. Trojanowska, M. 2010. Cellular and molecular aspects of vascular dysfunction in systemic sclerosis. *Nat. Rev. Rheumatol.* 6: 453–460.
6. Bhattacharyya, S., and J. Varga. 2015. Emerging roles of innate immune signaling and toll-like receptors in fibrosis and systemic sclerosis. *Curr. Rheumatol. Rep.* 17: 474.
7. Allanore, Y., O. Distler, M. Matucci-Cerinic, and C. P. Denton. 2018. Review: defining a unified vascular phenotype in systemic sclerosis. *Arthritis Rheumatol.* 70: 162–170.
8. Barnes, T. C., D. G. Spiller, M. E. Anderson, S. W. Edwards, and R. J. Moots. 2011. Endothelial activation and apoptosis mediated by neutrophil-dependent interleukin 6 trans-signalling: a novel target for systemic sclerosis? *Ann. Rheum. Dis.* 70: 366–372.
9. Kahaleh, B. 2008. Vascular disease in scleroderma: mechanisms of vascular injury. *Rheum. Dis. Clin. North Am.* 34: 57–71; vi.
10. Fleming, J. N., and S. M. Schwartz. 2008. The pathology of scleroderma vascular disease. *Rheum. Dis. Clin. North Am.* 34: 41–55; vi.

11. Eelen, G., P. de Zeeuw, L. Treps, U. Harjes, B. W. Wong, and P. Carmeliet. 2018. Endothelial cell metabolism. *Physiol. Rev.* 98: 3–58.
12. Mostmans, Y., M. Cutolo, C. Giddelo, S. Decuman, K. Melsens, H. Declercq, E. Vandecasteele, F. De Keyser, O. Distler, J. Gutermuth, and V. Smith. 2017. The role of endothelial cells in the vasculopathy of systemic sclerosis: a systematic review. *Autoimmun. Rev.* 16: 774–786.
13. Ramasamy, S. K., A. P. Kusumbe, and R. H. Adams. 2015. Regulation of tissue morphogenesis by endothelial cell-derived signals. *Trends Cell Biol.* 25: 148–157.
14. Miquerol, L., J. Thireau, P. Bideaux, R. Sturny, S. Richard, and R. G. Kelly. 2015. Endothelial plasticity drives arterial remodeling within the endocardium after myocardial infarction. *Circ. Res.* 116: 1765–1771.
15. Piera-Velazquez, S., Z. Li, and S. A. Jimenez. 2011. Role of endothelial-mesenchymal transition (EndoMT) in the pathogenesis of fibrotic disorders. *Am. J. Pathol.* 179: 1074–1080.
16. Xiao, L., and A. C. Dudley. 2017. Fine-tuning vascular fate during endothelial-mesenchymal transition. *J. Pathol.* 241: 25–35.
17. Kuwana, M., and Y. Okazaki. 2014. Brief report: impaired in vivo neovascularization capacity of endothelial progenitor cells in patients with systemic sclerosis. *Arthritis Rheumatol.* 66: 1300–1305.
18. Kuwana, M., and Y. Okazaki. 2012. Quantification of circulating endothelial progenitor cells in systemic sclerosis: a direct comparison of protocols. *Ann. Rheum. Dis.* 71: 617–620.
19. Altorok, N., Y. Wang, and B. Kahaleh. 2014. Endothelial dysfunction in systemic sclerosis. *Curr. Opin. Rheumatol.* 26: 615–620.
20. Manetti, M., E. Romano, I. Rosa, S. Guiducci, S. Bellando-Randone, A. De Paulis, L. Ibba-Manneschi, and M. Matucci-Cerinic. 2017. Endothelial-to-mesenchymal transition contributes to endothelial dysfunction and dermal fibrosis in systemic sclerosis. *Ann. Rheum. Dis.* 76: 924–934.
21. Zordan, P., E. Rigamonti, K. Freudenberg, V. Conti, E. Azzoni, P. Rovere-Querini, and S. Brunelli. 2014. Macrophages commit postnatal endothelium-derived progenitors to angiogenesis and restrict endothelial to mesenchymal transition during muscle regeneration. *Cell Death Dis.* 5: e1031.
22. Dowson, C., N. Simpson, L. Duffy, and S. O'Reilly. 2017. Innate immunity in systemic sclerosis. *Curr. Rheumatol. Rep.* 19: 2.
23. Higashi-Kuwata, N., M. Jinnin, T. Makino, S. Fukushima, Y. Inoue, F. C. Muchemwa, Y. Yonemura, Y. Komohara, M. Takeya, H. Mitsuya, and H. Ihn. 2010. Characterization of monocyte/macrophage subsets in the skin and peripheral blood derived from patients with systemic sclerosis. *Arthritis Res. Ther.* 12: R128.
24. Ciechomska, M., S. O'Reilly, S. Przyborski, F. Oakley, K. Bogunia-Kubik, and J. M. van Laar. 2016. Histone demethylation and toll-like receptor 8-dependent cross-talk in monocytes promotes transdifferentiation of fibroblasts in systemic sclerosis via Fra-2. *Arthritis Rheumatol.* 68: 1493–1504.
25. Wang, Y., M. Nakayama, M. E. Pitulescu, T. S. Schmidt, M. L. Bochenek, A. Sakakibara, S. Adams, A. Davy, U. Deutsch, U. Lüthi, et al. 2010. Ephrin-B2 controls VEGF-induced angiogenesis and lymphangiogenesis. *Nature* 465: 483–486.
26. Srinivas, S., T. Watanabe, C. S. Lin, C. M. William, Y. Tanabe, T. M. Jessell, and F. Costantini. 2001. Cre reporter strains produced by targeted insertion of EYFP and ECFP into the ROSA26 locus. *BMC Dev. Biol.* 1: 4.
27. Moeller, A., K. Ask, D. Warburton, J. Gauldie, and M. Kolb. 2008. The bleomycin animal model: a useful tool to investigate treatment options for idiopathic pulmonary fibrosis? *Int. J. Biochem. Cell Biol.* 40: 362–382.
28. van den Hoogen, F., D. Khanna, J. Fransen, S. R. Johnson, M. Baron, A. Tyndall, M. Matucci-Cerinic, R. P. Naden, T. A. Medsger, Jr., P. E. Carreira, et al. 2013. 2013 classification criteria for systemic sclerosis: an American College of Rheumatology/European League against Rheumatism collaborative initiative. *Arthritis Rheum.* 65: 2737–2747.
29. Ieronimakis, N., G. Balasundaram, and M. Reyes. 2008. Direct isolation, culture and transplant of mouse skeletal muscle derived endothelial cells with angiogenic potential. *PLoS One* 3: e0001753.
30. Corna, G., L. Campana, E. Pignatti, A. Castiglioni, E. Tagliafico, L. Bosurgi, A. Campanella, S. Brunelli, A. A. Manfredi, P. Apostoli, et al. 2010. Polarization dictates iron handling by inflammatory and alternatively activated macrophages. *Haematologica* 95: 1814–1822.
31. Patel, J., E. J. Seppanen, M. P. Rodero, H. Y. Wong, P. Donovan, Z. Neufeld, N. M. Fisk, M. François, and K. Khosrotehrani. 2017. Functional definition of progenitors versus mature endothelial cells reveals key SoxF-dependent differentiation process. *Circulation* 135: 786–805.
32. Braun, R. K., D. A. Ferrick, A. Sterner-Kock, P. J. Kilshaw, D. M. Hyde, and S. N. Giri. 1996. Comparison of two models of bleomycin-induced lung fibrosis in mouse on the level of leucocytes and T cell subpopulations in bronchoalveolar lavage. *Comparative Haematology International* 6: 141–148.
33. Hattori, N., J. L. Degen, T. H. Sisson, H. Liu, B. B. Moore, R. G. Pandrangi, R. H. Simon, and A. F. Drew. 2000. Bleomycin-induced pulmonary fibrosis in fibrinogen-null mice. *J. Clin. Invest.* 106: 1341–1350.
34. Lam, A. P., E. L. Herzog, D. Melichian, J. Sennello, Y. Gan, K. Raparia, R. Homer, A. Yeldandi, and J. Varga. 2016. Distinct patterns of pulmonary injury and fibrosis induced by intratracheal and subcutaneous bleomycin in the mouse: relevance for distinct forms of human lung fibrosis. In *Cystic and Idiopathic Pulmonary Fibrosis: Risk Factors, Management and Long-Term Health Outcomes*. L. Robertson, ed. Nova Science Publishers, Hauppauge, NY, p. 127–152.
35. Murray, L. A., T. L. Hackett, S. M. Warner, F. Shaheen, R. L. Argentieri, P. Dudas, F. X. Farrell, and D. A. Knight. 2008. BMP-7 does not protect against bleomycin-induced lung or skin fibrosis. *PLoS One* 3: e4039.
36. Manetti, M., S. Guiducci, E. Romano, S. Bellando-Randone, M. L. Conforti, L. Ibba-Manneschi, and M. Matucci-Cerinic. 2012. Increased serum levels and tissue expression of matrix metalloproteinase-12 in patients with systemic sclerosis: correlation with severity of skin and pulmonary fibrosis and vascular damage. *Ann. Rheum. Dis.* 71: 1064–1072.
37. Borghini, A., M. Manetti, F. Nacci, S. Bellando-Randone, S. Guiducci, M. Matucci-Cerinic, L. Ibba-Manneschi, and E. Weber. 2015. Systemic sclerosis sera impair angiogenic performance of dermal microvascular endothelial cells: therapeutic implications of cyclophosphamide. *PLoS One* 10: e0130166.
38. Fonteneau, G., C. Bony, R. Goulabchand, A. T. J. Maria, A. Le Quellec, S. Rivière, C. Jorgensen, P. Guilpain, and D. Noël. 2017. Serum-Mediated oxidative stress from systemic sclerosis patients affects mesenchymal stem cell function. *Front. Immunol.* 8: 988.
39. Pessina, P., Y. Kharraz, M. Jardí, S. Fukada, A. L. Serrano, E. Perdiguero, and P. Muñoz-Cánoves. 2015. Fibrogenic cell plasticity blunts tissue regeneration and aggravates muscular dystrophy. *Stem Cell Reports* 4: 1046–1060.
40. Walker, U. A., A. Tyndall, L. Czirják, C. Denton, D. Farge-Bancel, O. Kowal-Bielecka, U. Müller-Ladner, C. Bocelli-Tyndall, and M. Matucci-Cerinic. 2007. Clinical risk assessment of organ manifestations in systemic sclerosis: a report from the EULAR Scleroderma Trials and Research group database. *Ann. Rheum. Dis.* 66: 754–763.
41. DeCicco-Skinner, K. L., G. H. Henry, C. Cataisson, T. Tabib, J. C. Gwilliam, N. J. Watson, E. M. Bullwinkle, L. Falkenburg, R. C. O'Neill, A. Morin, and J. S. Wiest. 2014. Endothelial cell tube formation assay for the in vitro study of angiogenesis. *J. Vis. Exp.* DOI: 10.3791/51312.
42. Allanore, Y., R. Simms, O. Distler, M. Trojanowska, J. Pope, C. P. Denton, and J. Varga. 2015. Systemic sclerosis. *Nat. Rev. Dis. Primers* 1: 15002.
43. Chia, J. J., and T. T. Lu. 2015. Update on macrophages and innate immunity in scleroderma. *Curr. Opin. Rheumatol.* 27: 530–536.
44. Shi, C., and E. G. Pamer. 2011. Monocyte recruitment during infection and inflammation. *Nat. Rev. Immunol.* 11: 762–774.
45. Mantovani, A., A. Sica, and M. Locati. 2005. Macrophage polarization comes of age. *Immunity* 23: 344–346.
46. Novak, M. L., and T. J. Koh. 2013. Phenotypic transitions of macrophages orchestrate tissue repair. *Am. J. Pathol.* 183: 1352–1363.
47. Stifano, G., and R. B. Christmann. 2016. Macrophage involvement in systemic sclerosis: do we need more evidence? *Curr. Rheumatol. Rep.* 18: 2.
48. Nicolosi, P. A., E. Tombetti, N. Maugeri, P. Rovere-Querini, S. Brunelli, and A. A. Manfredi. 2016. Vascular remodelling and mesenchymal transition in systemic sclerosis. *Stem Cells Int.* 2016: 4636859.
49. Hashimoto, N., S. H. Phan, K. Imaizumi, M. Matsuo, H. Nakashima, T. Kawabe, K. Shimokata, and Y. Hasegawa. 2010. Endothelial-mesenchymal transition in bleomycin-induced pulmonary fibrosis. *Am. J. Respir. Cell Mol. Biol.* 43: 161–172.
50. Patel, A. S., A. Smith, S. Nucera, D. Biziato, P. Saha, R. Q. Attia, J. Humphries, K. Mattock, S. P. Grover, O. T. Lyons, et al. 2013. TIE2-expressing monocytes/macrophages regulate revascularization of the ischemic limb. *EMBO Mol. Med.* 5: 858–869.
51. Xu, X., X. Tan, B. Tampe, E. Sanchez, M. Zeisberg, and E. M. Zeisberg. 2015. Snail is a direct target of hypoxia-inducible factor 1α (HIF1α) in hypoxia-induced endothelial to mesenchymal transition of human coronary endothelial cells. *J. Biol. Chem.* 290: 16653–16664.
52. Chen, I. H., H. H. Wang, Y. S. Hsieh, W. C. Huang, H. I. Yeh, and Y. J. Chuang. 2013. PRSS23 is essential for the Snail-dependent endothelial-to-mesenchymal transition during valvulogenesis in zebrafish. *Cardiovasc. Res.* 97: 443–453.
53. Egorova, A. D., P. P. S. J. Khedoe, M.-J. T. H. Goumans, B. K. Yoder, S. M. Nauli, P. ten Dijke, R. E. Poelmann, and B. P. Hierck. 2011. Lack of primary cilia primes shear-induced endothelial-to-mesenchymal transition. *Circ. Res.* 108: 1093–1101.
54. Krizbai, I. A., Á. Gasparics, P. Nagyőszi, C. Fazakas, J. Molnár, I. Wilhelm, R. Bencs, L. Rosivall, and A. Sebe. 2015. Endothelial-mesenchymal transition of brain endothelial cells: possible role during metastatic extravasation. *PLoS One* 10: e0119655.
55. Dejana, E., and M. G. Lampugnani. 2018. Endothelial cell transitions. *Science* 362: 746–747.
56. Welch-Reardon, K. M., N. Wu, and C. C. W. Hughes. 2015. A role for partial endothelial-mesenchymal transitions in angiogenesis? *Arterioscler. Thromb. Vasc. Biol.* 35: 303–308.
57. Mendoza, F. A., S. Piera-Velazquez, J. L. Farber, C. Feghali-Bostwick, and S. A. Jiménez. 2016. Endothelial cells expressing endothelial and mesenchymal cell gene products in lung tissue from patients with systemic sclerosis-associated interstitial lung disease. *Arthritis Rheumatol.* 68: 210–217.
58. Capobianco, A., A. Monno, L. Cottone, M. A. Venneri, D. Biziato, F. Di Puppo, S. Ferrari, M. De Palma, A. A. Manfredi, and P. Rovere-Querini. 2011. Proangiogenic Tie2(+) macrophages infiltrate human and murine endometriotic lesions and dictate their growth in a mouse model of the disease. *Am. J. Pathol.* 179: 2651–2659.
59. Moritz, F., J. Schniering, J. H. W. Distler, R. E. Gay, S. Gay, O. Distler, and B. Maurer. 2017. Tie2 as a novel key factor of microangiopathy in systemic sclerosis. *Arthritis Res. Ther.* 19: 105.
60. Taroni, J. N., C. S. Greene, V. Martyanov, T. A. Wood, R. B. Christmann, H. W. Farber, R. A. Lafyatis, C. P. Denton, M. E. Hinchcliff, P. A. Pioli, et al. 2017. A novel multi-network approach reveals tissue-specific cellular modulators of fibrosis in systemic sclerosis. *Genome Med.* 9: 27.
61. Higashi-Kuwata, N., T. Makino, Y. Inoue, M. Takeya, and H. Ihn. 2009. Alternatively activated macrophages (M2 macrophages) in the skin of patient with localized scleroderma. *Exp. Dermatol.* 18: 727–729.
62. Khanna, D., C. P. Denton, A. Jahreis, J. M. van Laar, T. M. Frech, M. E. Anderson, M. Baron, L. Chung, G. Fierlbeck, S. Lakshminarayanan, et al.

2016. Safety and efficacy of subcutaneous tocilizumab in adults with systemic sclerosis (faSScinate): a phase 2, randomised, controlled trial. *Lancet* 387: 2630–2640.
63. Distler, O., and J. H. W. Distler. 2016. Tocilizumab for systemic sclerosis: implications for future trials. *Lancet* 387: 2580–2581.
64. Mantovani, A., S. K. Biswas, M. R. Galdiero, A. Sica, and M. Locati. 2013. Macrophage plasticity and polarization in tissue repair and remodelling. *J. Pathol.* 229: 176–185.
65. Dace, D. S., A. A. Khan, J. Kelly, and R. S. Apte. 2008. Interleukin-10 promotes pathological angiogenesis by regulating macrophage response to hypoxia during development. *PLoS One* 3: e3381.
66. Khanna, D., C. P. Denton, C. J. F. Lin, J. M. van Laar, T. M. Frech, M. E. Anderson, M. Baron, L. Chung, G. Fierlbeck, S. Lakshminarayanan, et al. 2018. Safety and efficacy of subcutaneous tocilizumab in systemic sclerosis: results from the open-label period of a phase II randomised controlled trial (faSScinate). *Ann. Rheum. Dis.* 77: 212–220.